

# Response of small sea ice floes in regular waves: A comparison of numerical and experimental results



Wei Bai<sup>a,b,\*</sup>, Tong Zhang<sup>b</sup>, David J. McGovern<sup>c</sup>

<sup>a</sup> School of Computing, Mathematics and Digital Technology, Manchester Metropolitan University, Chester Street, Manchester M1 5GD, UK

<sup>b</sup> Department of Civil and Environmental Engineering, National University of Singapore, Kent Ridge, Singapore 117576, Singapore

<sup>c</sup> Department of Civil, Environmental & Geomatic Engineering, University College London, Gower Street, London WC1E 6BT, UK

## ARTICLE INFO

### Keywords:

Ice floe  
Dynamic response  
Linear analysis  
Computational fluid dynamics  
Experimental study

## ABSTRACT

In severe seas ice floes can gain significant kinetic energy presenting a hazard to offshore structures and shipping. A numerical investigation is presented to investigate the kinematic response of sea ice floes in waves. The results are compared against available experimental data. The surge, heave and drift velocity are analyzed for various different ice floe shapes using the potential flow model HydroSTAR<sup>®</sup> and the viscous flow CFD model OpenFOAM<sup>®</sup>. The results show relative wavelength ( $\lambda$  normalized with floe length  $L_c$ )  $\lambda/L_c$  strongly influences heave and surge, with a heave resonance occurring at  $\lambda/L_c=8$  for the cubic floe not being correspondingly observed for the square floe. The heave Response Amplitude Operator (RAO) is found to increase with floe thickness with a resonance occurring when relative thickness  $b/L_c \geq 0.5$ . Shape is observed to be less important than thickness. At small values of  $\lambda/L_c$  the floe is observed to move forward over the whole wavelength resulting in its drift displacement. Both vertical velocity relative to theoretical particle velocity  $V_y/V_p$  and ratio of forward and backward velocities show resonance at  $\lambda/L_c=8$ . Comparing with experimental data, the linear analysis using HydroSTAR<sup>®</sup> overestimates the heave and surge RAOs. OpenFOAM<sup>®</sup>, however, appears to provide a much better agreement with the experimental data indicating viscosity plays an important role in floe kinematics.

## 1. Introduction

The trend in the decline of Arctic sea ice is predicted to lead to an ice-free Arctic Ocean by 2040 (Arctic Climate Impact Assessment (ACIA), 2004). Such seasonal reduction in sea ice coverage may open the North West Passage and Northern Sea Routes to shipping, greatly reducing the journey time between the Pacific and Atlantic Oceans. Additionally, according to a USGS (United States Geological Survey) survey between 13% and 30% of the world's untapped oil and gas are thought to be located beneath the Arctic Ocean (U.S. Geological Survey (USGS), 2008). The reduction in ice coverage is cause for increased interest in exploiting these reserves.

The Arctic is a particularly harsh environment and hazards to offshore and shipping operations include that of sea ice interactions (Thomson and Rogers, 2014). The loss of ice coverage will increase fetch and, in low concentrations, such as stretches of ocean adjacent to but not within the Marginal Ice Zone (MIZ), motions of a sea ice floe (floating ice block which is not attached to land) that is small with respect the dominant wavelength ( $\lambda$ ) will be driven by ocean waves and become significant in severe seas. The analysis of the problem is similar to that of a thin, free-floating body, and a detailed review is given in

McGovern and Bai (2014a). In the case of small fragments of sea ice, i.e., up to tens of meters in size and much smaller than the dominant wavelengths, the floe is essentially non-compliant (Meylan and Squire, 1994, 1996; McGovern and Bai, 2014a). In such a case flexural response of the floe is negligible and radiation damping is dominant. The floes may still cover a large region of many kilometres in length, but will be found in all different sizes down to small floes. Such small floes even in the MIZ are sensitive to full six degrees of freedom of motions from wave forcings (Frankenstein et al., 2001). Indeed such motions have been measured in the field on isolated glacial ice bergs of a variety of sizes (Wadhams et al., 1983). Understanding the kinematic response of a small ice floe in wave is, therefore, key to properly addressing the potential hazard that such a floe may have to offshore operations and shipping in the Arctic.

Due to its significance in cold regions engineering practice, there has been extensive research on drift motions of small ice floes. Initially, researchers focused more on the derivation of theoretical or semi-theoretical models to solve the simplified ice problems. For example, Rumer et al. (1979) extended the Morison's equation to calculate the drift motion of small floating object in a gravity wave field. Shen and Ackley (1991) used a one-dimensional model to study collisions

\* Corresponding author at: School of Computing, Mathematics and Digital Technology, Manchester Metropolitan University, Chester Street, Manchester M1 5GD, UK.  
E-mail address: [w.bai@hotmail.com](mailto:w.bai@hotmail.com) (W. Bai).

between ice floes and herding using the slope-sliding model proposed in Rumer et al. (1979). Shen and Zhong (2001) found that wave reflection has a profound effect on the drift pattern. Even for a very small reflection coefficient, the floating object can stop its propagation after some time. This trapping phenomenon depends on the added mass and drag coefficients. Marchenko (1999) independently derived a similar slope-sliding theory as in Rumer et al. (1979). Grotmaack and Meylan (2006) related the two theories in Marchenko (1999), Shen and Zhong (2001) and identified an error in the derivation of Rumer et al. (1979). Recently, Huang et al. (2016) presented an improved analytical solution to the drift of small rigid floating objects of arbitrary shapes under regular waves.

Apart from the two comprehensive reviews in Squire et al. (1995) and Squire (2007) where a large amount of research on the interaction of sea ice and ocean waves in the MIZ have been summarised, many experiments and theoretical studies have been carried out to study the response of small floating objects in waves. Arunachalam et al. (1987) analyzed the short term motion of icebergs in linear waves both theoretically and experimentally. Lever et al., (1988a, 1988b) and Huang et al. (2011) studied different factors which can affect the motion and drift velocity of small icebergs experimentally. However, it can be seen that most attention has focused on glacial icebergs, which are now well understood. Attention, including the works of Meylan and Squire (1994, 1996) and Meylan (2002), has focused on the flexural response of thin floating bodies in waves. Of interest here is how the compliant properties of the floes affect floe kinematic and reflection response.

More recently, Montiel et al., (2013a, 2013b) presented measurements of the oscillatory motions of thin plastic disk in regular waves, and compared the measurements with predictions of the potential flow model. Bennetts and Williams (2015) presented measured surge, heave and pitch motions of a solitary wooden disk at a subset of the incident wave frequencies and amplitudes used for their tests. Their model was based on a combined potential flow and thin plate theory, and the assumption of linear motions. Both a low-concentration array in which discs were separated by approximately one disk diameter in equilibrium, and a high-concentration array in which adjacent discs were almost touching in equilibrium, were considered in their experiments. Meylan et al. (2015a) presented measurements of the surge, heave and pitch motions of a thin plastic disk as a function of  $\lambda$ . They showed that the model predictions in their study are accurate for incident  $\lambda$  approximately greater than two times floe diameter. Meylan et al. (2015b) tested the motions of two different plate models with distinct material properties in regular waves by using the thin plate model. The results indicated that the motions of floes are essentially linear.

In order to further understand kinematics of ice floes in water waves, McGovern and Bai (2014a) conducted an experiment in a wave flume to investigate in detail the kinematic and dynamic response of ice floes, their drift velocity, the influence of body geometry, thickness and other parameters. They concluded that the ice floe's motion can be affected by its own properties such as shape and thickness and also the wave properties such as wavelength. Additional discussion on ice floe interaction and impact characteristics with a single fixed vertical cylinder was given in McGovern and Bai (2014b). They studied the effect of a single cylinder on the upstream, near-cylinder, impact and post impact kinematics and velocities of floes of various shapes in a variety of wave conditions. This paper is, therefore, the follow-up of our previous work on ice floe kinematics. As the experimental data presented in McGovern and Bai (2014a) was not sufficiently validated due to the lack of published data in the public domain, one aim of the present paper is to reproduce the physical experiment numerically, so that the accuracy of both our experiment and the present numerical study in the kinematics of ice floes can be firmly verified by the comprehensive comparison between the numerical and experimental results. Also, different numerical tools are compared and recommendations are made.

However, the literature review shows that CFD work on the kinematics of ice floes in water waves is very rare. Therefore, identifying a suitable numerical tool for the ice floe problem is another aim of the present paper. Two different numerical tools are chosen to carry out the numerical simulation: the linear analysis based on the potential flow theory by the software HydroSTAR<sup>®</sup> and the computational fluid dynamic (CFD) simulation based on the viscous flow theory by the open source tool OpenFOAM<sup>®</sup>. OpenFOAM<sup>®</sup>, with the advantage of being free and open source, has been adopted to solve many problems in coastal and offshore engineering. In the study of Higuera et al. (2013a, 2013b), the OpenFOAM<sup>®</sup> was adopted to simulate several coastal processes such as wave breaking and wave interaction with obstacle. Chen et al. (2014) also used this CFD tool to study wave interaction with a vertical cylinder. Both of these two studies indicated that the OpenFOAM<sup>®</sup> is accurate and promising. After testing three validation cases, Morgan et al. (2010) and Morgan and Zang (2011) concluded that OpenFOAM<sup>®</sup> may potentially be a very useful tool for researchers and engineers in coastal and offshore engineering. To simulate water waves, Jacobsen et al. (2012) extended OpenFOAM<sup>®</sup> with a wave generation and absorption method. Furthermore, Higuera et al., (2013a, 2013b) implemented the specific boundary conditions for realistic wave generations and presented a robust three-dimensional, two-phase numerical model for practical applications in coastal engineering.

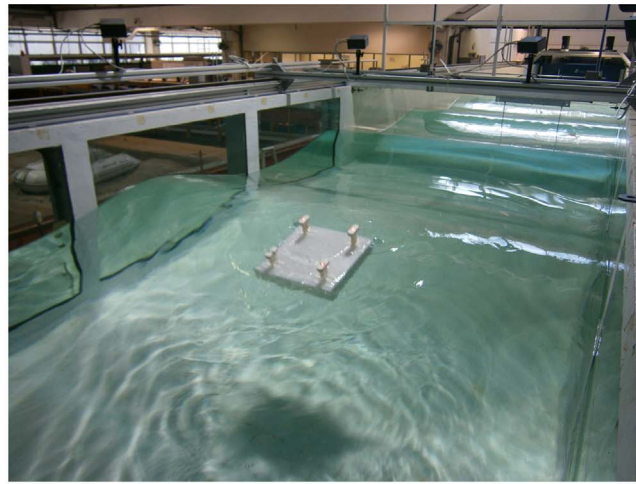
## 2. Experimental study

### 2.1. Experiment setup

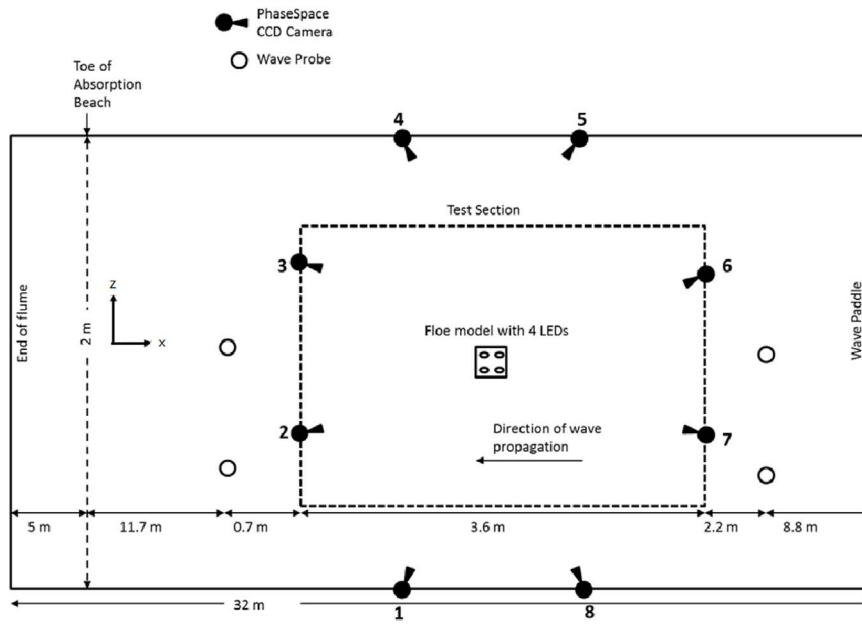
The experimental set-up is described in detail in McGovern and Bai (2014a) and as such, is given here in brief. The flume used is the 32 m long 2 m wide wave flume situated in the Hydraulic Engineering Laboratory at the National University of Singapore. An effective absorption beach was located at the end of the flume. Extensive testing during the construction of the flume showed that the beach reflects < 5% of incident wave height, and this was confirmed by additional testing before the current experimental campaign in McGovern and Bai (2014a). Sea ice models of various shapes are formed from paraffin wax (density  $\rho=890 \text{ kg m}^{-3}$ ). The kinematic response of the models in regular waves is measured using a PhaseSpace Improv motion tracking system, see Fig. 1a. This system tracks the full six-degrees-of-freedom of motion of the floe models in the test section. Free surface elevation is recorded using four resistance-type wave gauges up and downstream of the test section (Fig. 1b). The system consisted of 8 cameras mounted on a frame around the test section supported by the flume walls. The cameras are able to resolve the LED to 0.1 mm at a distance of 5 m. The LEDs were positioned at equidistant points from each corner of the ice model. The system was calibrated using a calibration wand on which LEDs are fixed at known distance apart. The accuracy of the system is rated at 1% of the distance between the cameras and the measured LED (see McGovern and Bai (2014a) for more details).

### 2.2. Data processing

Raw data obtained in the experiments is the time series record of displacement in the  $x$  and  $y$  directions. The solid line in Fig. 2 shows the raw data of  $x$  displacement, which cannot be used directly for the analysis of surge motion due to the presence of the drift motion. According to the engineering practice, the surge motion refers to the periodically oscillating component in the  $x$  displacement. Therefore, to obtain the surge motion the effect of drift motion should be separated from the time series record. It should be noted that due to the different processing procedure, the surge motion defined in McGovern and Bai (2014a) is slightly different to the conventional definition of surge motion widely adopted in engineering practice, since the drift motion is not completely removed from the results of surge motion. Here, to be in



(a)



(b)

Fig. 1. a) Image of a floe model with attached LED lights undergoing testing in regular waves and b) a schematic diagram of the flume.

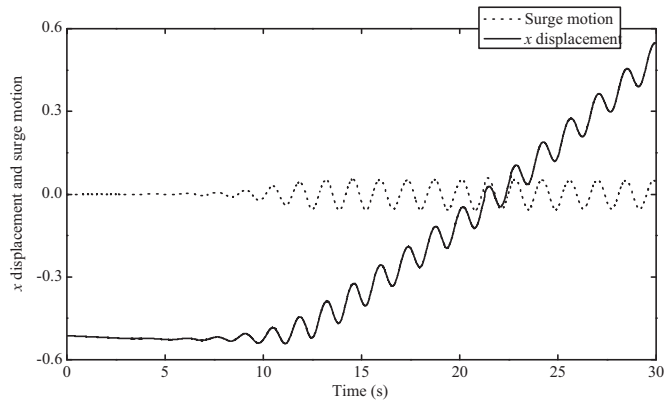


Fig. 2. An example of x displacement trace in experiment and corresponding surge motion after processing.

line with the conventional definition of surge motion, the mean value of x displacement at each time instant is calculated by averaging the displacement around this time instant over one wave period. The oscillating surge motion is eventually obtained by removing the mean at each time instant from the measured signal. By using this processing procedure, the oscillating component can be separated from the motion in the x direction, as shown by the dashed line in Fig. 2, which can be defined as the surge motion of moving body. The same approach will also be adopted in the following sections to process the numerical results.

In addition, since the large drift motion is a specific phenomenon associated with ice floes in waves, the drift velocity is a key physical property that is of great engineering significance when studying ice impact problems (Huang et al., 2011). Generally, the constant drift velocity in the quasi-steady state can be computed by two approaches (Huang et al., 2011). One is to obtain the instantaneous mean velocity within one wave period based on an up-crossing method that is widely used in analyzing irregular waves. In this method, the period-averaged mean drift velocity is a function of time, and can be calculated by dividing the horizontal displacement between two neighboring peaks

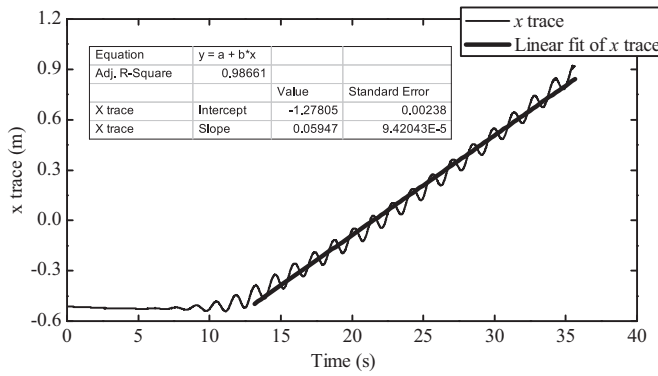


Fig. 3. An illustration of determination of drift velocity  $V_d$  using the best-fitting linear line approach.

by the wave period. The other method is to calculate the mean drift velocity in the quasi-steady stage by determining the slope of a best-fitting linear trend line, which is adopted in this study. For the purpose of demonstration, Fig. 3 shows the  $x$  displacement trace for a typical case in the experiment, and the corresponding best-fitting linear trend line from 15 s to 35 s marked by a thick solid line. The information regarding the performance of the approach is also shown in a small table embedded in the figure. The drift velocity  $V_d$  can be easily determined by calculating the slope of the best-fitting line. In the case shown in the figure, the drift velocity  $V_d$  is 0.05947 m/s.

### 3. Linear numerical analysis

There exist various numerical models ranging from the simplified linear potential flow model to the more complete computational fluid dynamic simulations, which are available for the numerical simulation of response of ice floes in water waves. However, each numerical model has its own advantages and disadvantages due to various assumptions made and inherent natures of the model. In this study, we mainly focus on two popular numerical models, and evaluate the performance of these two models.

#### 3.1. Linear diffraction/radiation method

The fluid is assumed to be incompressible and inviscid, and the motion irrotational. The water wave problem can be formulated in terms of a velocity potential  $\phi(x, y, z, t)$ , which satisfies Laplace's equation within the fluid domain surrounding the ice floe (Chen et al., 2015),

$$\nabla^2 \phi = 0, \tag{1}$$

and is subject to the boundary conditions applied on the ice floe surfaces given as:

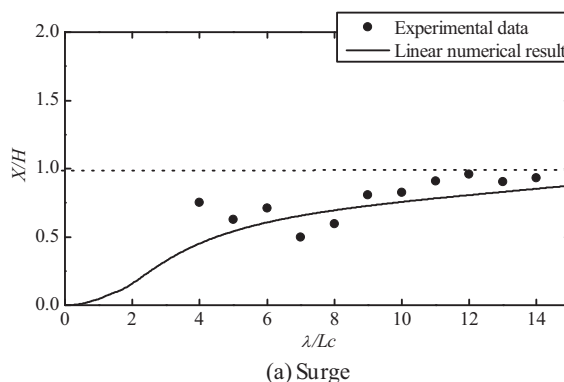


Fig. 4. Comparison of surge (a) and heave (b) RAOs of cube between the linear analysis and experiment.

$$\frac{\partial \phi}{\partial n} = V_n, \tag{2}$$

where  $n$  is the normal unit vector pointing out of the fluid domain, and  $V_n$  the normal velocity component of the solid surfaces. On the water surface, the first order boundary condition is

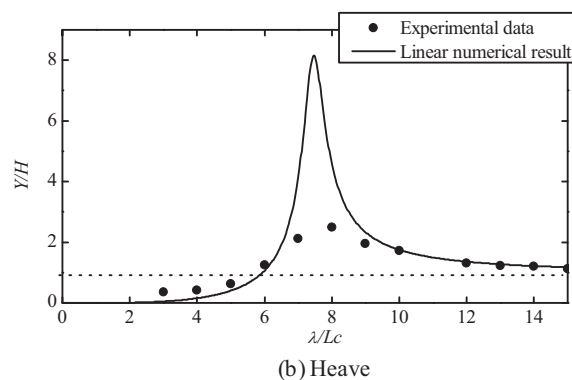
$$\frac{\partial^2 \phi}{\partial t^2} + g \frac{\partial \phi}{\partial z} = 0, \tag{3}$$

where  $g$  is the acceleration due to gravity. In addition, a suitable radiation condition on the outer boundary should be imposed to avoid the wave reflection from the far-field boundary.

This boundary value problem has been successfully solved in many widely used commercial software packages. In this study, the software package HydroSTAR<sup>®</sup> is adopted, which provides a complete solution of the first order problem of wave diffraction and radiation. The main output includes the wave forces and moments, wave elevation and dynamic response of floating bodies. As for the problem of ice floes in water waves investigated in the present study, this linear analysis tool is applied to simulate a cube of length 20 cm, and a square plate of length 30 cm and thickness 5 cm, in order to examine the capability of the linear analysis for this thin ice floe problem. The assumption of  $kL_c = O(1)$  is applicable for the potential flow model, where  $k$  is the wave number and  $L_c$  is the typical body length. After the mesh convergence test, the numbers of panels in the  $x$ ,  $y$  and  $z$  directions are chosen to be 8, 8 and 8 for the cube in the calculation, while the numbers of panels for the square plate are 18, 18 and 6. Due to the symmetry of the computational domain, only a quarter of the body is considered in the calculation, so that there are in total 80 and 189 panels on the cube and square plate surfaces, respectively.

#### 3.2. Numerical results and discussions

Our experimental results reveal that ice floe kinematics can be affected by incident wave height  $H$  and wavelength  $\lambda$ . However, in the linear analysis RAO (Response Amplitude Operator) of bodies is independent with incident wave height. We, therefore, can only study the influence of wavelength on the dynamic response of ice floes in waves. To make a direct comparison with our experiments, the wavelength is varied from 1.0m to 3.0 m for the cube and from 0.6m to 3.0 m for the square plate, as in the experiments. The linear analysis can directly provide the surge and heave RAOs, where the effect of drift is excluded. The numerical results are compared with the experimental data measured at the wave steepness  $H/\lambda$  of 0.02 for the cube and 0.044 for the square plate, as shown in Figs. 4 and 5 respectively. From the comparison of surge and heave RAOs of the cube as a function of relative wavelength  $\lambda/L_c$ , it can be seen that the surge RAO is in acceptable agreement, but the numerical simulation over-predicts the heave response by four times that of the experimental measurement at the peak frequency around  $\lambda/L_c = 7-9$ . Here,  $L_c$  is defined as the length



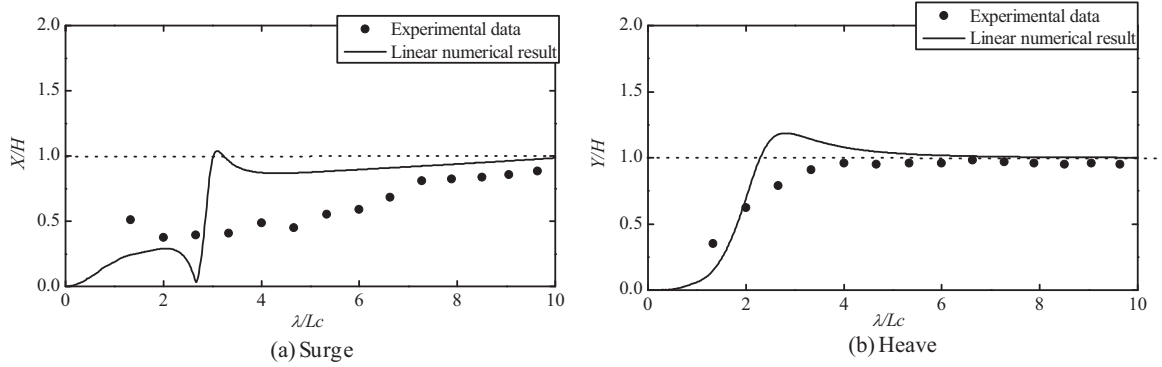


Fig. 5. Comparison of surge (a) and heave (b) RAOs of square plate between the linear analysis and experiment.

of the edge in horizontal plane for the square plate and the length of the edge for the cube respectively. For the square plate in Fig. 5, the numerical results reveal that the linear analysis seems to over-predict both the surge and heave RAOs. An unreasonable peak appears in both the surge and heave RAOs at about  $\lambda/L_c=3$ , whose value exceeds 1. Therefore, in the regime where  $\lambda/L_c$  is between 2 and 4, the linear analysis can be considered to provide inaccurate results for the square plate considered here.

Generally speaking, although with the similar trend, the linear analysis by HydroSTAR<sup>®</sup> is not able to provide good agreement with the experimental results, especially in the resonance range for the heave motion of the cube. The over-prediction of the numerical simulation is mainly due to the neglect of fluid viscosity in the potential flow model, which is verified later in Figs. 9 and 10 by the numerical results obtained using the viscous flow solver OpenFOAM<sup>®</sup> where the viscosity of fluid is considered. It is unsurprising that the results obtained by the linear potential flow analysis cannot agree with the experimental results well, as it is known that this theory is only valid for certain range of body size relative to wavelength. The only damping in the potential flow model is due to radiation damping, while as in the experimental case, viscous damping appears to play a more significant role in accurately predicting the dynamic responses. In addition to the assumptions made in the potential flow model, the linearization might be another source of error in the linear analysis. At the same time, as the commercial software HydroSTAR<sup>®</sup> can only provide the results in the frequency domain, which means the information about the displacement trace and the drift velocity that are the significant physical properties when studying ice floes in water waves, is missing. The advantage of the linear analysis is efficiency; the simulation can finish in a very short period of time. For a particular case, full RAO can be obtained on a normal workstation in 10 min when 500 wave frequencies are considered. However, to obtain more accurate numerical results with detailed information, a computational fluid dynamic simulation with the nonlinearity and fluid viscosity being taken into account is necessary.

#### 4. Computational fluid dynamic (CFD) simulation

##### 4.1. Mathematical formulation

The governing equations for viscous flows are the Reynolds averaged Navier-Stokes equations (Ferziger and Peric, 2012) within the domain surrounding the ice floe:

$$\frac{\partial \rho}{\partial t} + \frac{\partial}{\partial x_j}(\rho u_j) = 0, \quad (4)$$

$$\frac{\partial}{\partial t}(\rho u_i) + \frac{\partial}{\partial x_j}(\rho u_j u_i) = -\frac{\partial p}{\partial x_i} + \frac{\partial}{\partial x_j} \left[ \mu_e \left( \frac{\partial u_j}{\partial x_i} + \frac{\partial u_i}{\partial x_j} \right) \right] + \rho g_i, \quad (5)$$

where  $x_j$  ( $j=1, 2, 3$ ) represents the coordinate components,  $u_j$  is the

fluid velocity,  $p$  is the pressure,  $\rho$  is the fluid density.  $\mu_e = \mu + \mu_f$ , where  $\mu$  is the fluid viscosity and  $\mu_f$  is the turbulent eddy viscosity. In order to close the above governing equations, the two-equation  $k-\varepsilon$  turbulence model is adopted to simulate the turbulent flows:

$$\frac{\partial}{\partial t}(\rho k) + \frac{\partial}{\partial x_j}(\rho u_j k) = \frac{\partial}{\partial x_j} \left[ \left( \mu + \frac{\mu_f}{\delta_k} \right) \frac{\partial k}{\partial x_j} \right] + P_k - \rho \varepsilon, \quad (6)$$

$$\frac{\partial}{\partial t}(\rho \varepsilon) + \frac{\partial}{\partial x_j}(\rho u_j \varepsilon) = \frac{\partial}{\partial x_j} \left[ \left( \mu + \frac{\mu_f}{\delta_\varepsilon} \right) \frac{\partial \varepsilon}{\partial x_j} \right] + C_1 P_k \frac{\varepsilon}{k} - \rho C_2 \frac{\varepsilon^2}{k}, \quad (7)$$

$$P_k = \mu_f \left( \frac{\partial u_j}{\partial x_i} + \frac{\partial u_i}{\partial x_j} \right) \frac{\partial u_i}{\partial x_j}, \quad (8)$$

where  $\mu_f = C_\mu \rho k^2 / \varepsilon$ ,  $k$  is the turbulent kinetic energy,  $\varepsilon$  is the turbulent energy dissipation rate,  $\delta_k$  and  $\delta_\varepsilon$  are the turbulent Schmidt numbers. The constants in the turbulence model are set as  $C_\mu=0.09$ ,  $C_1=1.44$ ,  $C_2=1.92$ ,  $\delta_k=1.0$  and  $\delta_\varepsilon=1.33$ .

Volume of Fluid method (VOF) (Hirt and Nichols, 1981) is adopted to capture the air-water interface (the free water surface). In this method, the fraction of water volume existing in each computational element (known as the volume fraction) is advected by solving the following transport equation:

$$\frac{\partial \alpha}{\partial t} + \frac{\partial}{\partial x_j}(u_j \alpha) = 0, \quad (9)$$

where  $\alpha$  is the volume fraction of water. The volume fraction is used as the weighting factor to predict the fluid properties in each computational element,

$$\rho = \alpha \rho_w + (1 - \alpha) \rho_a, \quad (10)$$

$$\mu = \alpha \mu_w + (1 - \alpha) \mu_a, \quad (11)$$

where the subscripts  $w$  and  $a$  represent the corresponding fluid property of water and air respectively. It should be noted that on the body surface, the non-slip boundary condition is applied.

##### 4.2. Numerical implementation of OpenFOAM<sup>®</sup>

The CFD calculations are carried out using an open source CFD software, OpenFOAM<sup>®</sup> (Open Source Field Operation and Manipulation) which was first released in 2004. OpenFOAM<sup>®</sup> is essentially a C++ library that is used to create solvers for various fluid flow problems. OpenFOAM<sup>®</sup> comes with a great number of solvers but its open source nature can also enable users write their own solvers. Jacobsen et al. (2012) developed a solver, called Waves2Foam, to deal with the wave generation and wave-structure interaction problems. While this solver doesn't include the dynamic mesh utility in OpenFOAM<sup>®</sup> and as a result cannot deal with floating bodies. In the present study, Waves2Foam is coupled with the dynamic mesh function embedded in another OpenFOAM<sup>®</sup> solver, called

WaveDyMFOam, such that the moving body problems can be solved in the frame of Waves2FOam.

Three different types of floes are considered in the CFD calculations using OpenFOAM<sup>®</sup>: the first two are the cube and square plate that have been defined before in the linear analysis, and the last geometry is a regular triangle plate of length 30 cm and thickness 5 cm. The present study mainly investigates the effect of wavelength on ice floe kinematics, by varying the wavelength from about 0.6 m to 3.0m for all these three geometries. In the simulation of the cube, the wave steepness is set to  $H/\lambda=0.02$ , as used in the experiments. However, the wave steepness  $H/\lambda$  remains to be 0.044 for both the square and triangle plates, which was also adopted in the experiments for the same geometries. Various wave heights are also tested for the square plate with the same wavelength to study the influence on the drift velocity. The effect of ice floe thickness is also studied by a series tests for the square plate. Therefore, in total 54 test cases are run using OpenFOAM<sup>®</sup>.

In the numerical simulations, BlockMesh, a mesh type in OpenFOAM<sup>®</sup> which is very suitable for regular geometries, is used to discretize the computational domain for the cube and square plate, where the total numbers of elements are 400,000 and 432,000 respectively. For the triangle plate, because of the relatively irregular shape of the body SnappyHexMesh, another mesh type in OpenFOAM<sup>®</sup> which is more robust for irregular geometries, is used and 571,802 elements are adopted in the simulations. It should be noted that a coarser mesh of 200,000 elements and a finer mesh of 800,000 elements have also been tested for the cube to validate the feature of mesh convergence (not shown here). The calculations at those three meshes reveal that the intermediate mesh of 400,000 elements and the finer mesh can provide very agreeable results that deviate from those obtained at the coarser mesh, indicating that the results presented below at the adopted mesh is convergent in terms of computational mesh. In addition, non-uniform mesh is used for all the three geometries with suitable mesh refinement around the free surface and body surface. With 400,000 elements, one simulation for a duration of 30 s and a particular  $\lambda/L_c$  takes about 3–4 h in OpenFOAM<sup>®</sup> using 8 computer processors. In this study, our main focus is on the global dynamic motion of bodies in waves, rather than the detailed turbulent flow structures. Therefore, no special consideration has been given to the treatment of flow boundary layer. In Fig. 6, an example mesh is shown for a floating square plate generated in OpenFOAM<sup>®</sup>. Table 1 shows the wave properties and model shapes of simulations in OpenFOAM<sup>®</sup>.

## 5. CFD and experimental results

### 5.1. Time series of response

Time series of body response is a direct output in both the numerical simulation and experimental measurement. Fig. 7 shows

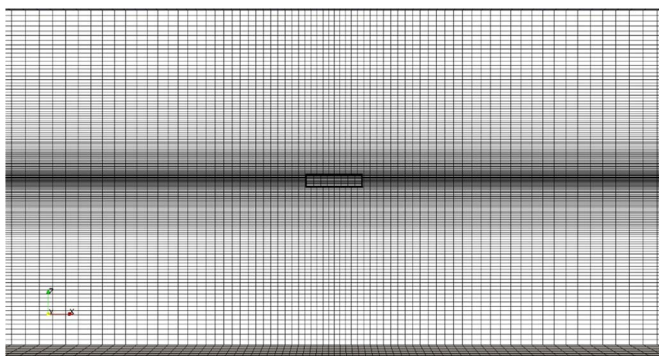


Fig. 6. The example mesh in OpenFOAM<sup>®</sup> for ice floe problem.

**Table 1**  
Summary of OpenFOAM<sup>®</sup> simulations.

| Number of runs  | $\lambda$ (m) | $H$ (m)       | $H/\lambda$   | $\lambda/L_c$ |
|---|---------------|---------------|---------------|---------------|
| Cubic model ( $L_c=20$ ) with different wavelengths                             |               |               |               |               |
| 11  | 1–3.0         | 0.02–0.06     | 0.02          | 5–15          |
| Square plate ( $L_c=30$ $b=5$ ) with different wavelengths                      |               |               |               |               |
| 12  | 0.4–3.0       | 0.0176–0.132  | 0.044         | 1.333–10      |
| Triangle plate ( $L_c=30$ $b=5$ ) with different wavelengths                    |               |               |               |               |
| 8   | 0.4–2.6       | 0.0176–0.1144 | 0.044         | 1.333–8.667   |
| Square plate ( $L_c=30$ $b=5$ ) with different wave heights                     |               |               |               |               |
| 8   | 1.8           | 0.02–0.16     | 0.0111–0.0899 | 6             |
| Square plate ( $L_c=30$ cm) with different thickness $b=7.5, 10, 15, 20, 30$ cm |               |               |               |               |
| 4   | 0.8           | 2.0           | 0.15          | 0.02          |

the displacements in the  $x$  and  $y$  directions and the comparison between the numerical results and experimental data for the square plate over five wave periods after the steady state has been achieved. The steady state means both the surge and heave motions become periodic with constant amplitudes and the drift component becomes a fixed value in each wave period. In this case, the wavelength  $\lambda=3$  m and wave height  $H=0.132$  m are considered. As shown in the figure, the ice floe experiences a periodic motion around the free surface in the  $y$  direction, whereas a clear drift can be observed although it also moves forwards and backwards periodically in the  $x$  direction. The comparison between the numerical results and experimental data shows that good agreement can be obtained for the surge and heave motions. To better demonstrate the body motion, the trajectory of the square plate moving in waves is shown in Fig. 8, from which we can see that the trajectory exhibits like a helix line rather than a closed line. The  $x$  displacement is periodic, but also involves a drifting component.

### 5.2. Effect of wavelength

In the tests of Lever et al. (1988a) for the iceberg motions, it was concluded that wavelength  $\lambda$  is a significant factor to influence the iceberg motions. In their experiments, four model geometries were adopted to study the effect of geometry on dynamic responses of icebergs. For a particular geometry, the influence of wavelength on body motions was also investigated. The results demonstrated that cylinder and cube models show a peak in the heave RAO at  $\lambda/L_c=6$  and then tend to be around 1 at larger  $\lambda/L_c$ , while the sphere and trapezoid show no peak. In this study, we first present our numerical and experimental results of surge and heave RAOs for the cube and compare with the experimental data in Lever et al. (1988a), as shown in Fig. 9, to validate both our numerical model and experiment. For the 20 cm cubic model, in McGovern and Bai (2014a) the test case was repeated for 6 times at each wave condition. The error bars of the experimental data are shown in Fig. 9, from which we can see that the errors of the experiments are small (less than 8%). We can also see from the figure that the surge and heave RAOs show different trend with the increase of relative wavelength  $\lambda/L_c$  for the cube. The surge RAO shows a constant increase with the wavelength, and after  $\lambda/L_c=10$  it approaches to 1, indicating the particle-like behavior of the ice floe. A peak appears in the heave RAO at around  $\lambda/L_c=8$ ; the heave motion decreases and tends to approach to 1 while increasing the wavelength so that the cube behaves like a water particle, in both the numerical, present and Lever et al.'s experimental results. Schwerdtfeger (1980) used a rectangular iceberg and assumed the motion only in the vertical cross-section. The frequencies of both linear and angular oscillations of a floating iceberg in the vertical plane were shown to converge to a certain value with the increase of body size in the horizontal plane. It was found that the heave resonance of an iceberg with straight sides

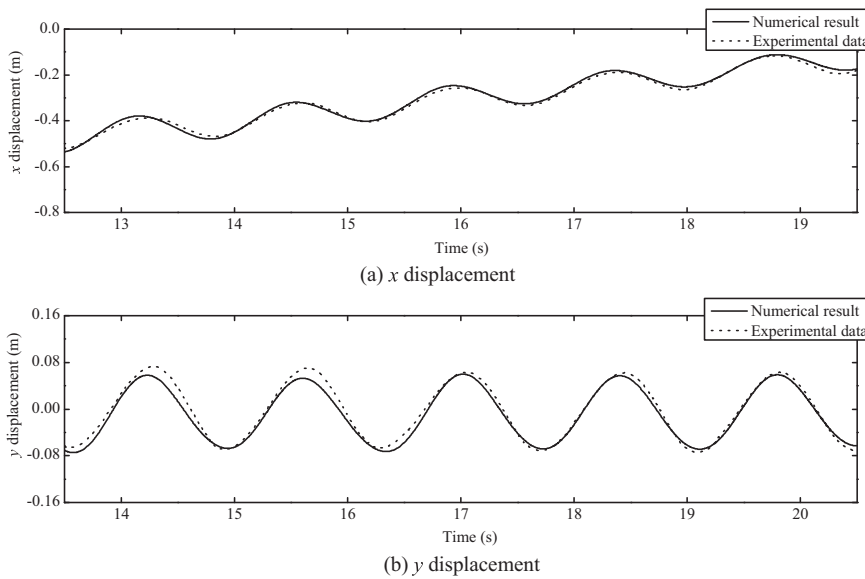


Fig. 7. Numerical and experimental results of time series of  $x$  (a) and  $y$  (b) displacements for the square plate.

can be easily computed by assuming linear oscillations:

$$\left(\frac{\lambda}{h}\right)_{res} = 2\pi \frac{\rho_i}{\rho_w} (1 + m_c), \tag{12}$$

where  $h$  is the thickness of the iceberg,  $m_c$  is the added mass coefficient in heave,  $\rho_i$  and  $\rho_w$  are the densities of ice and water respectively. The added mass coefficient for the cube in this case can be determined approximately by the formula  $ma=0.7\rho a^3$ , as shown in Blevins and Plunkett (1980). With this added mass coefficient, Eq. (12) shows that the heave resonance occurs at  $\lambda/L_c=9.7$  for the ice cube, which agrees with the numerical and experimental results shown in Fig. 9. This probably can also explain the lack of resonance in the heave for the square plate, as shown later. Eq. (12), at the same time, demonstrates that the thickness of the ice might be another important parameter, which will be further discussed later in detail.

Further observation of Fig. 9 reveals that the numerical result of surge motion is slightly different from the present experimental data, but closer to the data in Lever et al. (1988a). On the other hand, the heave motion in the numerical simulation experiences a larger peak compared to the experimental results, which may be due to the other damping influences (such as the surface roughness of the ice floe and the tank walls) in the experiments that cannot be taken into account in the numerical simulations. However, in general the present numerical simulation is able to provide accurate surge and heave RAOs, and the present experimental results are also in good agreement with numerical and Lever et al.'s experimental results.

Fig. 10 shows the surge and heave RAOs of the square plate in the present numerical simulation and physical experiment both with the wave steepness of  $H/\lambda=0.044$ . As seen in the figure, it is distinguishable from the cube case that there is no obvious peak observed in the heave RAO, but the surge RAO shows the similar characteristics with the cube case. It seems that the thickness of ice floe can affect the occurrence of

the resonance phenomenon in the heave motion, which will be further discussed later. A small discrepancy can still be observed for  $\lambda/L_c < 3$  in both heave and surge RAOs, which may be attributed to the small wave height (about 2 cm) adopted in both the numerical and experimental studies. The wave height is small in order to retain a constant wave steepness for these short waves. This may cause errors in both the experiments and numerical simulations.

Furthermore, with considering the over-prediction and unrealistic peak in the linear analysis, as shown in Figs. 4 and 5, the CFD simulations can obtain much better results than the linear analysis, which is reflected by the better agreement with the experimental data, especially for the cube case. As discussed before, the over-prediction in the linear analysis is due to the linear nature and the omission of the fluid viscosity in the basic assumptions of the linear potential flow model. Therefore, compared to the CFD simulation, the linear analysis may not be very suitable in accurately modeling the motion of floating ice floes, even though it is very efficient in computer time.

At the same time, the physical experiment also observes the phenomenon of green water appeared when  $\lambda/L_c < 5$  for the square plate. Green water is a quantity of water on the topside surface of body as a result of wave actions. The same green water is also noticed in the numerical simulations, whereas the critical value for the occurrence of this phenomenon is found to be around  $\lambda/L_c=4$ . Fig. 11 shows the test cases with and without the green water observed at  $\lambda/L_c=4$  and  $\lambda/L_c=10$  respectively for the square plate at the wave steepness  $H/\lambda=0.044$ . This green water effect may be one of the reasons for smaller surge and heave motions at smaller wavelengths. This phenomenon agrees with the findings in Skene et al. (2015), where a theoretical model of overwash of a floating plate was presented and validated by laboratory experiments. They also showed that overwash generally occurs for waves with relatively short lengths. For the cases with  $\lambda/L_c < 4$ , the relative error of the numerical simulation is larger and the reason

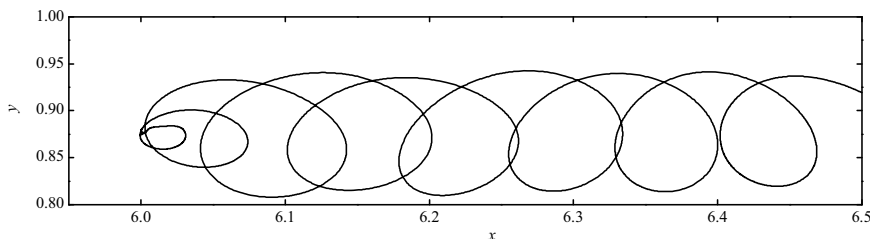


Fig. 8. Numerical result of trajectory of the square plate in waves.

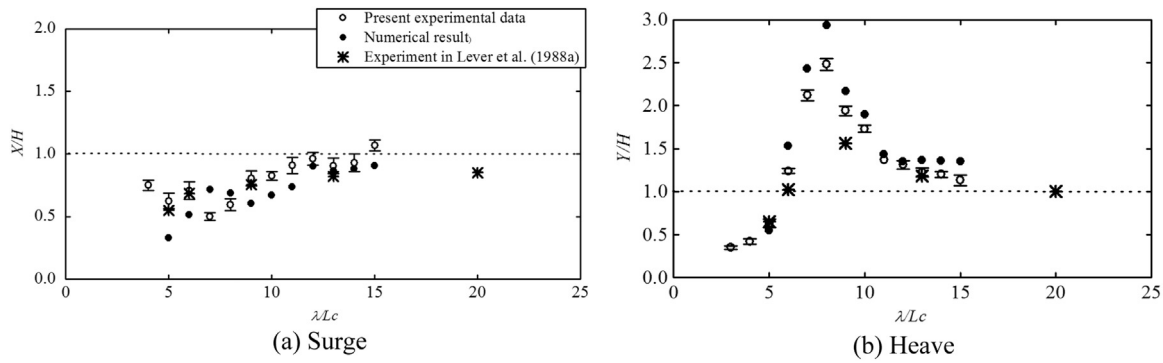


Fig. 9. Comparison of surge (a) and heave (b) RAOs of the cube between the present numerical and experimental results, and the experimental data in Lever et al. (1988a).

has been discussed. For the cases with  $\lambda/L_c > 4$ , the relative error is less than 10% which means that the numerical results are reliable.

5.3. Effect of model shape

In the physical experiments, a series of ice floes with different shapes have been tested. In the CFD simulations, three model shapes are chosen to test the hydrodynamic performance of different bodies. For the influence of other body shapes, see McGovern and Bai (2014a) for more details. The three body shapes chosen include the cube, square plate and triangle plate with streamline normal to one edge of the triangle. Fig. 12 shows the surge and heave RAOs of different body shapes obtained by both the numerical simulations and experiments. As seen in the figure, the surge motion presents an increasing trend with the increase of wavelength for all the three body shapes, and the numerical results are in good agreement with the experimental results. While for the heave RAO, results for different body shapes show great difference. For the cube, both the numerical and experimental results show a peak approximately at  $\lambda/L_c=8$ , where the heave response can reach more than two times that of the wave height  $H$ . For the square and triangle plates, there is no obvious heave resonance. Generally, for all the three body shapes, the numerical results show the same trend with the experimental data. However, the numerical results seem to underestimate the heave RAO for both the square and triangle plates when the wavelength is small. For the cases with  $\lambda/L_c < 4$ , the relative errors of heave RAOs are relatively large especially for the cube and square plate. While for the cases with  $\lambda/L_c > 4$ , the relative errors of all the three models are less than 10% except for the cube with  $\lambda/L_c=8$ . As for surge RAO, also the cube model shows the largest relative errors while the errors of all the three models are in a reasonable range.

5.4. Ice floe velocity

The velocity of ice floe is an important parameter when calculating ice impact force on structures by using the Morison equation (Wong and Sego, 1989). In the numerical simulation, the velocity of floating

body can be exported directly, while in the physical experiment the velocity can be calculated from the time series of body displacement. Fig. 13 shows a comparison of time series of velocities in the  $x$  and  $y$  directions between the numerical and experimental results for the square plate with the wavelength  $\lambda=3$  m and wave height  $H=0.132$  m. It can be seen that the  $x$  velocity in the positive  $x$  direction is obviously larger than that in the negative direction, which indicates the occurrence of the body drift in the  $x$  direction. For the heave velocity, the maximum upward and downward velocities are approximately the same. When the steady state is reached, the maximum  $x$  and  $y$  velocities of the square plate predicted by the numerical simulation agree reasonably well with the experimental results.

Fig. 14 shows the  $x$  and  $y$  velocities,  $V_x$  and  $V_y$ , of the cube normalized by the corresponding theoretical water particle velocity  $V_p$  as a function of the relative wavelength  $\lambda/L_c$ . Here,  $V_x$  and  $V_y$  refer to the maximum velocities in the  $x$  and  $y$  directions respectively, and  $V_p$  is defined as:

$$V_{px} = \frac{H}{2} \sigma \frac{\cosh k(h+z)}{\sinh kh} \cos(kx - \sigma t) \tag{13}$$

$$V_{py} = \frac{H}{2} \sigma \frac{\sinh k(h+z)}{\sinh kh} \cos(kx - \sigma t) \tag{14}$$

As shown in the figure, the horizontal relative velocity  $V_x/V_p$  varies around 1 but shows no specific trend. The vertical relative velocity  $V_y/V_p$  demonstrates the same trend as in the heave RAO with a resonance happened at approximately  $\lambda/L_c=8$ . As for comparison, the numerical results agree with the experimental results well in  $V_y/V_p$ . However,  $V_x/V_p$  is smaller than the experimental results but with a similar trend. Furthermore, with the increase of  $\lambda/L_c$  the ratio of the horizontal positive and negative velocities is also shown in Fig. 15. As can be seen in the figure, the general trends of the numerical simulation and experiment are the same. The ratio shows a peak at  $\lambda/L_c=8$  and with the increase of  $\lambda/L_c$ , the ratio approaches an asymptotic value of 1.5.

For the cube, there is always a horizontal negative velocity at all the relative wavelengths investigated, which indicates that the cube moves forwards and backwards. However, for the square plate, the physical

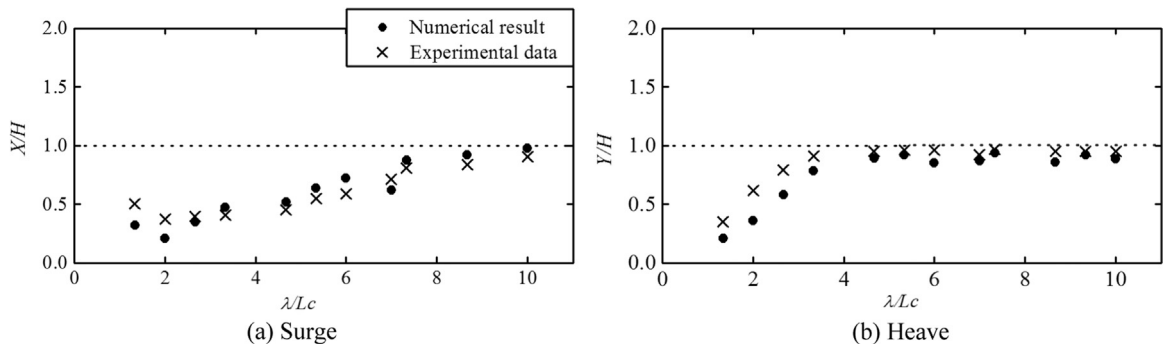
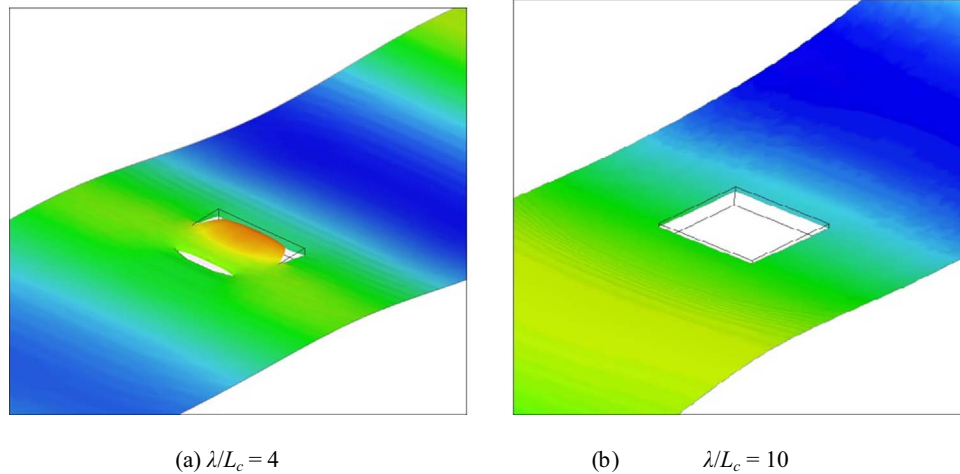
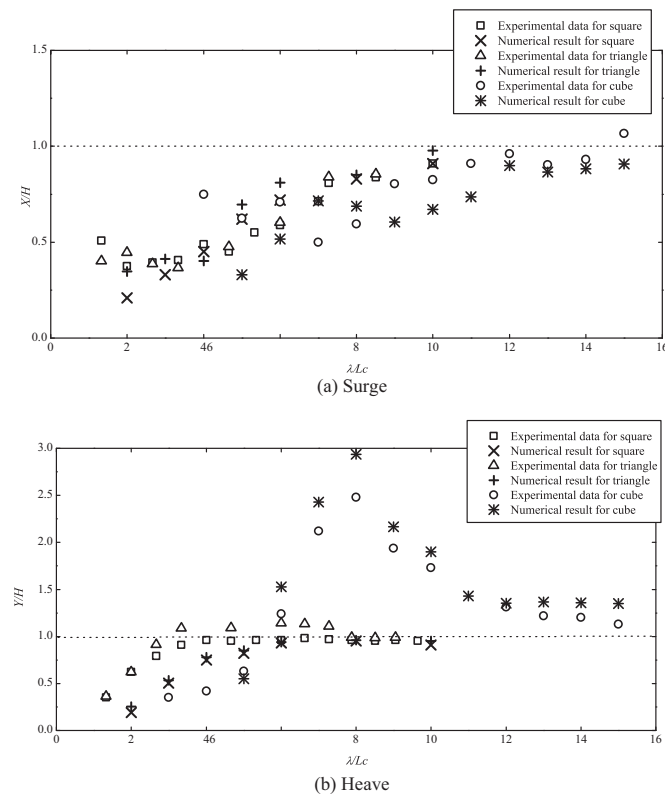


Fig. 10. Comparison of surge (a) and heave (b) RAOs of the square plate between the present numerical and experimental results.



**Fig. 11.** The 3D free surface profile around the square plate for  $\lambda/L_c=4$  (a) with green water and  $\lambda/L_c=10$  (b) without green water. (For interpretation of the references to color in this figure, the reader is referred to the web version of this article.)



**Fig. 12.** Comparison of surge (a) and heave (b) RAOs of three different body shapes between the present numerical and experimental results.

experiment shows that the horizontal negative velocity does not appear at small wavelengths when  $\lambda/L_c < 5.3$ . In this situation, the floe keeps moving forwards all the time without any backward motion. The same phenomenon is also observed in the present numerical simulation when  $\lambda/L_c < 4$ . This is because drift velocity becomes dominant when  $\lambda/L_c$  is small. Fig. 16 shows the numerical results of surge displacement for the square plate at  $\lambda/L_c=2$  and 5. With constant wave steepness, the larger wavelength implies that a higher wave was used in the simulation. Without the obvious backward velocity, the floe moves even faster at  $\lambda/L_c=2$  with a smaller wave height compared to that at  $\lambda/L_c=5$ . This indicates that the drift velocity  $V_d$  does not necessarily increase with the wave height, but is affected more by the relative wavelength.

To visualize the velocity in the domain, Fig. 17 shows the velocity

field around the cube with the relative wavelength  $\lambda/L_c=13$  and wave height  $H=0.052$  m at two time instants. In Fig. 17(a), the wave crest passes the cube at  $t=10.3$  s, while the wave trough passes the cube at  $t=10.9$  s in Fig. 17(b). When the wave crest passes, the velocity of most water particles around the body is pointing upwards and forwards so that the body also moves in that direction. However, when the wave trough passes, the velocity of most particles around the body is in the opposite direction, the body therefore moves downwards and backwards.

### 5.5. Drift velocity

For a pure wave motion in fluid dynamics, the Stokes drift velocity is the average velocity when following a specific fluid parcel as it travels with the fluid flow. In the Lagrangian description, fluid parcels may drift far from their initial positions. The equation of the drift velocity is given as follow:

$$V_d = \frac{ga^2k^2 \cosh 2k(h+z)}{\omega \sinh 2kh}, \tag{15}$$

where  $a$  is the wave amplitude,  $\omega$  is wave frequency.

According to Eq. (15), we can see that the solution is a quadratic function of the  $ka$  number. In the present study, the wavelength is constant at  $\lambda=1.8$  m and the wave height is varied in order to achieve the desired range of  $ka$  numbers. Fig. 18 shows the numerical results of drift velocity for the square plate normalized by the wave celerity  $C$  as a function of  $ka$  number, together with the experimental results of both the present study for the same square plate and Huang et al. (2011) for the square plate of length 20 cm and thickness 4.5 cm. The drift velocity obtained by the Stokes wave theory is also included in the figure for clearer demonstration. Both the numerical and experimental results are slightly larger than the theoretical results as shown in Fig. 18 while they are generally in good agreement.

### 5.6. Effect of thickness

The present experimental data has shown that the floe thickness  $b$  has a dramatic effect on floe motions, especially in the heave direction. Fig. 19 shows the numerical and experimental results of heave RAO for the square plate with two different thicknesses,  $b=5$  cm and  $b=7.5$  cm. With increasing of  $\lambda/L_c$ , the heave RAO in both the numerical and experimental results seems to approach the value of 1. The floe with larger thickness has a larger heave response. The experimental results of the square plate with larger thickness also demonstrate that a heave resonance appears, although it is not very obvious. The numerical

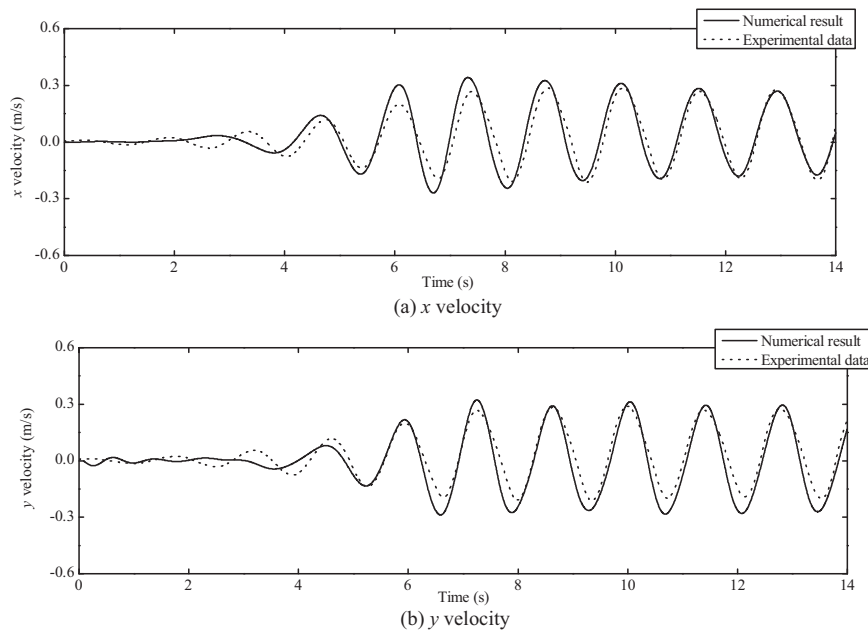


Fig. 13. Time series of  $x$  (a) and  $y$  (b) velocities obtained by both the numerical simulation and experiment for the square plate with  $\lambda=3$  m and  $H=0.132$  m.

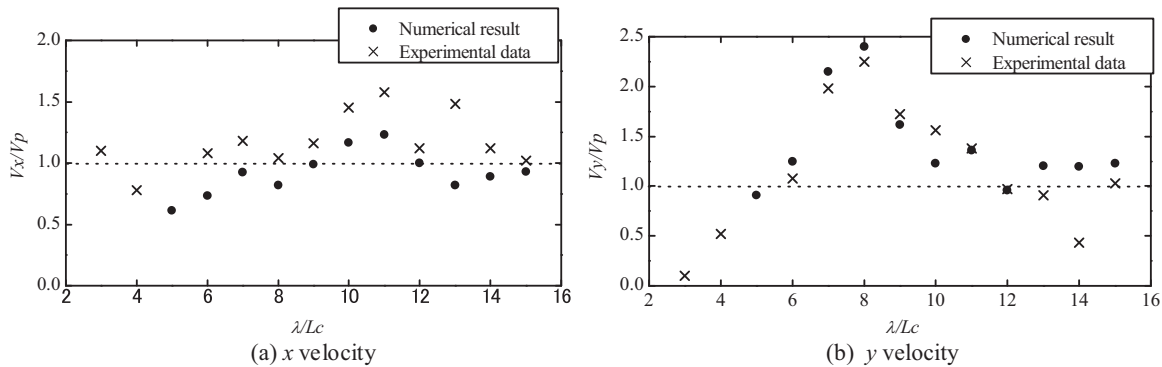


Fig. 14. Comparison of numerical and experimental results of  $x$  (a) and  $y$  (b) velocities normalized by the theoretical water particle velocity for the cube.

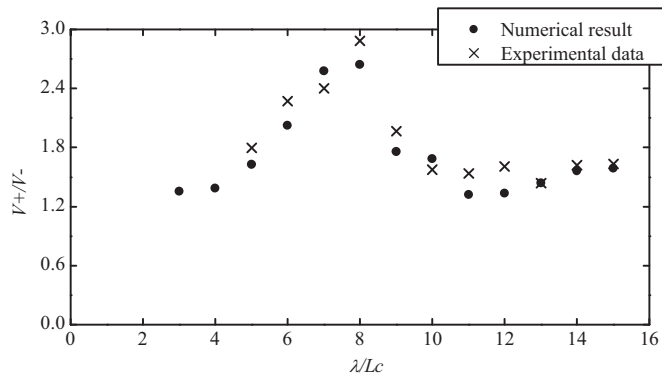


Fig. 15. Comparison of numerical and experimental results of the ratio of horizontal positive and negative velocities for the cube as a function of relative wave length.

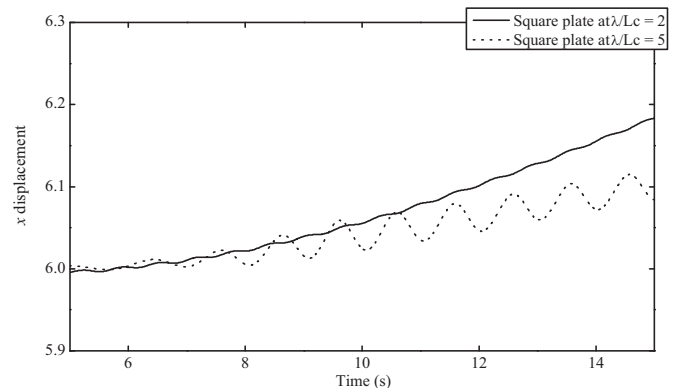


Fig. 16. Numerical result of displacement in the  $x$  direction for the square plate at  $\lambda/L_c=2$  and 5.

results seem to follow the same trend as the experimental data, but underestimate the heave RAO, as seen before. The square plate with thickness larger than 7.5 cm is not further investigated in the experiment, as the aim of the experiment is to study the motion of sea ice floes with small thicknesses.

As discussed before, the cube has shown an obvious heave resonance at about  $\lambda/L_c=8$ . To further investigate this more numerical tests are run for a square plate of length 30 cm with various thicknesses ranging from 5 cm to 30 cm, allowing for the systematic analysis of the

effect of thickness as it changes gradually from a square plate to a cube. Fig. 20 shows the numerical result of heave response of those square plates with various floe thicknesses  $b$ . We can see from the figure that when the thickness  $b \geq 15$  cm or the relative thickness  $b/L_c \geq 0.5$ , the heave RAO shows an obvious resonance, and with the thickness increasing, the heave resonance turns to be more and more significant.

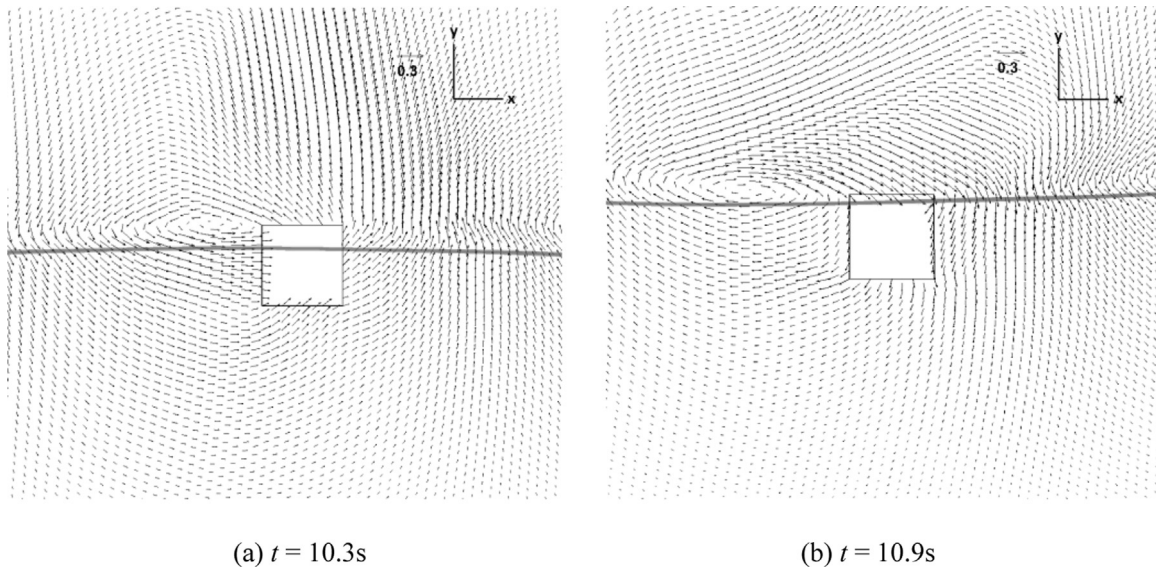


Fig. 17. Velocity field around the cube with  $\lambda/L_c=13$  and  $H=0.052$  m at two time instants: (a)  $t=10.3$  s and (b)  $t=10.9$  s.

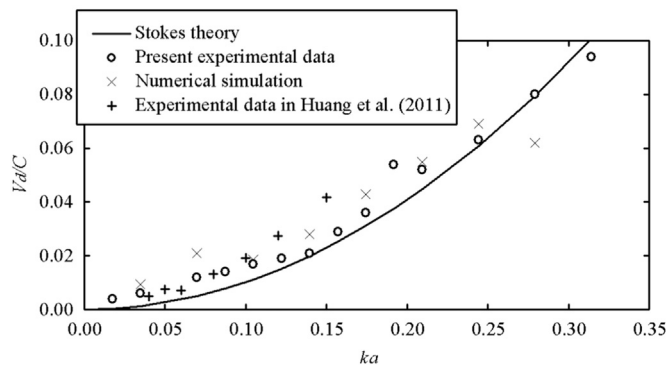


Fig. 18. Numerical result of drift velocity for the square plate and comparison with the experimental results of both the present study and Huang et al. (2011).

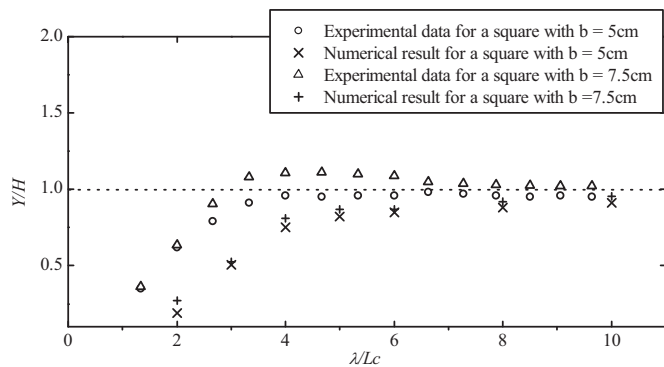


Fig. 19. Numerical and experimental heave RAOs for the square plate with two different thicknesses,  $b=5$  cm and  $b=7.5$  cm.

6. Conclusion

A series of physical model tests are conducted to study response of small ice floes in regular water waves. Since this experiment addresses the research gap in the small ice floe kinematics, a numerical simulation of the same problem is necessary to validate the experimental results. Additionally, due to the high demand for resources and time consuming nature of the experiment, finding a reliable numerical tool is vital for the problem of small ice floes in water waves. To achieve this purpose, the linear analysis based on the potential flow model and

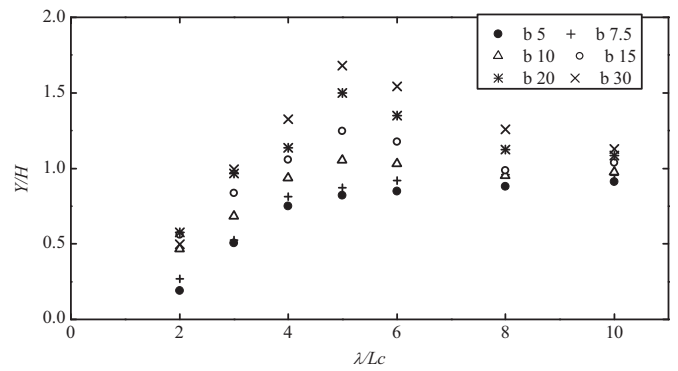


Fig. 20. Numerical result of heave response of square plates with variable floe thicknesses  $b$ .

the CFD simulation based on the viscous flow model are adopted and compared with the experimental data. Many distinct characteristics associated with kinematics of small ice floes in waves are identified in both the numerical and experimental studies.

The relative wavelength  $\lambda/L_c$  is found to have dramatic effect on the heave and surge RAOs. The heave resonance occurs for the cube at approximately the relative wavelength  $\lambda/L_c=8$ , whereas for the square plate only an increasing trend is observed in the heave response. The present numerical simulation reveals that the heave RAO increases with the floe thickness, and the heave resonance appears at the relative thickness  $b/L_c \geq 0.5$ . The square and triangle plates with the same thickness  $b$  show minimal difference in the heave and surge motions. In the vertical direction the maximum upward and downward velocities are approximately the same. However, in the horizontal direction the maximum forward velocity is larger than the backward velocity and the difference causes the drift displacement. Both the vertical relative velocity  $V_y/V_p$  and the ratio of the forward and backward velocities in the horizontal direction  $V_x/V$  show a resonance at  $\lambda/L_c=8$ . No backward velocity is observed when the relative wavelength  $\lambda/L_c$  is relatively small for the square plate; the floe moves forwards all the time. In addition to the comparison with the experimental results, to show the factor which affects the resonance, several additional cases other than that in the experiments are simulated to show the trend of body motions from non-resonance to resonance.

The linear results obtained by HydroSTAR<sup>®</sup> seem to overestimate the surge and heave RAOs especially for the cube when the resonance occurs in the range of  $\lambda/L_c=6$  to 9, probably because the nature of

linear potential flow model adopted in HydroSTAR<sup>®</sup>. The inaccuracy can also be observed for the square plate considered here in the regime where  $\lambda/Lc=2$  to 4. In general, the open source CFD software OpenFOAM<sup>®</sup> can provide much better agreement with the experimental data than the linear analysis. Extensive CFD simulations and comparisons with the experimental data reveal that the numerical results obtained by OpenFOAM<sup>®</sup> are reasonably accurate, except for the underestimation of the heave RAO for the square plate. The comparison shown in this study indicates that the fluid viscosity is an important parameter which cannot be ignored at laboratory scale when investigating the response of small ice floes in water waves.

## References

- Arctic Climate Impact Assessment (ACIA), 2004. Impacts of a Warming Arctic. Cambridge University Press, Cambridge, UK.
- Arunachalam, V.M., Murray, J.J., Mugeridge, D.B., 1987. Short term motion analysis of icebergs in linear waves. *Cold Reg. Sci. Technol.* 13, 247–258.
- Bennetts, L.G., Williams, T.D., 2015. Water wave transmission by an array of floating discs. *Proc. R. Soc. Lond. A: Math. Phys. Eng. Sci.* 471 (2173), 20140698.
- Blevins, R.D., Plunkett, R., 1980. Formulas for natural frequency and mode shape. *J. Appl. Mech.* 47, 461.
- Chen, L.F., Zang, J., Hillis, A.J., Morgan, G.C.J., Plummer, A.R., 2014. Numerical investigation of wave–structure interaction using OpenFOAM. *Ocean Eng.* 88, 91–109.
- Chen, X.B., Liu, H.X., Duan, W.Y., 2015. Semi-analytical solutions to wave diffraction of cylindrical structures with a moonpool with a restricted entrance. *J. Eng. Math.* 90 (1), 51–66.
- Ferziger, J.H., Peric, M., 2012. *Computational Methods for Fluid Dynamics*. Springer Science & Business Media, New York, USA.
- Frankenstein, S., Loset, S., Shen, H.H., 2001. Wave-ice interactions in the Barents sea marginal ice zone. *J. Cold Reg. Eng.* 15 (2), 91–102.
- Grotmaack, R., Meylan, M.H., 2006. Wave forcing of small floating bodies. *J. Waterw. Port Coast. Ocean Eng.* 132 (3), 192–198.
- Higuera, P., Lara, J.L., Losada, I.J., 2013a. Realistic wave generation and active wave absorption for Navier–Stokes models: application to OpenFOAM<sup>®</sup>. *Coast. Eng.* 71, 102–118.
- Higuera, P., Lara, J.L., Losada, I.J., 2013b. Simulating coastal engineering processes with OpenFOAM<sup>®</sup>. *Coast. Eng.* 71, 119–134.
- Hirt, C.W., Nichols, B.D., 1981. Volume of fluid (VOF) method for the dynamics of free boundaries. *J. Comput. Phys.* 39 (1), 201–225.
- Huang, G., Wing-Keung, A.L., Huang, Z., 2011. Wave-induced drift of small floating objects in regular waves. *Ocean Eng.* 38, 712–718.
- Huang, G., Huang, Z.H., Law, A.W., 2016. Analytical study on drift of small floating objects under regular waves. *J. Eng. Mech.* 142 (6), 06016002.
- Jacobsen, N.G., Fuhrman, D.R., Fredsøe, J., 2012. A wave generation toolbox for the open-source CFD library: OpenFoam<sup>®</sup>. *Int. J. Numer. Methods Fluids* 70 (9), 1073–1088.
- Lever, J.H., Attwood, D., Sen, D., 1988a. Factors affecting the prediction of wave-induced iceberg motion. *Cold Reg. Sci. Technol.* 15, 177–190.
- Lever, J.H., Reimer, E., Diemand, D., 1988b. A model study of the wave-induced motion of small icebergs and bergy bits. *J. Offshore Mech. Arct. Eng.* 110, 101–107.
- Marchenko, A.V., 1999. The floating behaviour of a small body acted upon by a surface wave. *J. Appl. Math. Mech.* 63 (3), 471–478.
- McGovern, D.J., Bai, W., 2014a. Experimental study on kinematics of sea ice floes in regular waves. *Cold Reg. Sci. Technol.* 103, 15–30.
- McGovern, D.J., Bai, W., 2014b. Experimental study of wave-driven impact of sea ice floes on a circular cylinder. *Cold Reg. Sci. Technol.* 108, 36–48.
- Meylan, M.H., 2002. Wave response of an ice floe of arbitrary geometry. *J. Geophys. Res.* 107 (C1), 3005.
- Meylan, M.H., Yiew, L.J., Bennetts, L.G., French, B.J., Thomas, G.T., 2015a. Surge motion of an ice floe in waves: comparison of theoretical and experimental models. *Ann. Glaciol.* 56 (69), 107–111.
- Meylan, M.H., Bennetts, L.G., Cavaliere, C., Alberello, A., Toffoli, A., 2015b. Experimental and theoretical models of wave-induced flexure of a sea ice floe. *Phys. Fluids* 27 (4), 041704.
- Meylan, M.H., Squire, V.A., 1994. The response of ice floes to ocean waves. *J. Geophys. Res.* 99 (C1), 899–900.
- Meylan, M.H., Squire, V.A., 1996. Response of a circular ice floe to ocean waves. *J. Geophys. Res.* 101 (C4), 8869–8884.
- Montiel, F., Bennetts, L.G., Squire, V.A., Bonnefoy, F., Ferrant, P., 2013a. Hydroelastic response of floating elastic disks to regular waves. Part 2: Modal analysis. *J. Fluid Mech.* 723, 629–652.
- Montiel, F., Bonnefoy, F., Ferrant, P., Bennetts, L.G., Squire, V.A., Marsault, P., 2013b. Hydroelastic response of floating elastic disks to regular waves. Part 1: Wave tank experiments. *J. Fluid Mech.* 723, 604–628.
- Morgan, G., Zang, J., 2011. Application of OpenFOAM to coastal and offshore modelling. In: *Proceedings of 26th International Workshop of Water Wave and Floating Bodies*, Athens, Greece.
- Morgan, G., Zang, J., Greaves, D., Heath, A., Whitlow, C., Young, J., 2010. Using the rasInterFoam CFD model for wave transformation and coastal modelling. In: *Proceedings of 32nd Conference on Coastal Engineering*. Shanghai, China.
- Rumer, R.R., Crissman, R.D., Wake, A., 1979. Ice transport in great lakes. Great Lakes Environmental Research Laboratory, National Oceanic and Atmospheric Administration, US Dept. of Commerce.
- Schwerdtfeger, P., 1980. Iceberg oscillation and ocean waves. *Ann. Glaciol.* 1, 63–65.
- Shen, H.H., Ackley, S.F., 1991. A one-dimensional model for wave-induced ice-floe collisions. *Ann. Glaciol.* 15, 87–95.
- Shen, H.H., Zhong, Y., 2001. Theoretical study of drift of small rigid floating objects in wave fields. *J. Waterw. Port Coast. Ocean Eng.* 127 (6), 343–351.
- Skene, D.M., Bennetts, L.G., Meylan, M.H., Toffoli, A., 2015. Modelling water wave overwash of a thin floating plate. *J. Fluid Mech.* 777, R3.
- Squire, V.A., 2007. Of ocean waves and sea-ice revisited. *Cold Reg. Sci. Technol.* 49, 110–133.
- Squire, V.A., Dugan, J.P., Wadhams, P., Rottier, P.J., Liu, A.K., 1995. Of ocean waves and sea-ice. *Ann. Rev. Fluid Mech.* 27, 115–168.
- Thomson, J., Rogers, W.E., 2014. Swell and sea in the emerging Arctic Ocean. *Geophys. Res. Lett.* 41 (9), 3136–3140.
- U.S. Geological Survey (USGS), 2008. Circum-Arctic Resource Appraisal: Estimates of Undiscovered Oil and Gas North of the Arctic Circle. U.S. Geological Survey Fact Sheet 2008-3049.
- Wadhams, P., Kristensen, M., Orheim, O., 1983. The response of Antarctic icebergs to ocean waves. *J. Geophys. Res.* 88, 6053–6065.
- Wong, T.T., Sego, D.C., 1989. Design requirement for ice forces. *Can. Geotech. J.* 26 (4), 524–535.